Microseismic monitoring of meso-scale stimulations for the DOE EGS Collab project at the Sanford Underground Research Facility

Martin Schoenball[1], Jonathan Ajo-Franklin[1], Doug Blankenship[2], Paul Cook[1], Patrick Dobson[1], Yves Guglielmi[1], Pengcheng Fu[3], Timothy Kneafsey[1], Hunter Knox[2], Petr Petrov[1], Michelle Robertson[1], Paul Schwering[2], Dennise Templeton[3], Craig Ulrich[1], Todd Wood[1], and the EGS Collab Team[*]

[1] Lawrence Berkeley National Laboratory, One Cyclotron Rd, Berkeley, CA, 94720, USA
[2] Sandia National Laboratory
[3] Lawrence Livermore National Laboratory

schoenball@lbl.gov

Keywords: EGS Collab, mesoscale experiments, microseismic monitoring

ABSTRACT

The U.S. Department of Energy's Enhanced Geothermal System (EGS) Collab project aims to improve our understanding of hydraulic stimulations in crystalline rock for enhanced geothermal energy production through execution of intensely monitored meso-scale experiments. The first experiment is being performed at the 4850 ft level of the Sanford Underground Research Facility (SURF), approximately 1.5 km below the surface at Lead, South Dakota.

Here we report on microseismic monitoring of repeated stimulation experiments and subsequent flow tests between two boreholes in the Poorman Formation. Stimulations were performed at several locations in the designated injection borehole at flow rates from 0.1 to 5 L/min over temporal durations from minutes to hours. Microseismic monitoring was performed using a dense 3D sensor array including two cemented hydrophone strings with 12 sensors at 1.75 m spacing accompanied by 18 3-C accelerometers, deployed in 6 monitoring boreholes, completely surrounding the stimulation region. Continuous records were obtained over a two-month period using a novel dual recording system consisting of a conventional 96 channel exploration seismograph and a high-performance 64 channel digitizer sampling sensors at 4 and 100 kHz respectively.

Using a standard STA/LTA triggering algorithm, we detected thousands of microseismic events with recorded energy in a frequency range generally above 3 kHz and up to 40 kHz. The locations of these events are consistent with creation of a hydraulic fracture and additional reactivation of pre-existing structures. Using manual pick refinement and double-difference relocation we are able to track the fracture growth to high precision. We estimate the times and locations of the fracture intersecting a monitoring and the production borehole using microseismic events. They are in excellent agreement with independent measurements using distributed temperature sensing, in-situ strain observations and measurements of conductivity changes.

1. INTRODUCTION

The U.S. Department of Energy's EGS Collab experiment Enhanced Geothermal System (EGS) Collab project (see Kneafsey et al., 2019 and references therein) aims to improve our understanding of hydraulic stimulations in crystalline rock for enhanced geothermal energy production through execution of intensely-monitored meso-scale experiments. The first experiment is being performed at the 4850 ft level of the Sanford Underground Research Facility (SURF), approximately 1.5 km below the surface at Lead, South Dakota. Knowledge gained during the EGS Collab experiments is intended to be applied to full-scale experiments as well as commercial EGS deployments.

In Experiment 1, the objective is to improve our capabilities to understand the formation of hydraulic fractures through an integrated experimental and modelling effort. The experimental site is located adjacent to the site of the kISMET experiment (Oldenburg et al., 2017). The host rock is the Poorman formation, which is a metamorphic rock of phyllite composition (Frash et al., 2019). Common to crystalline rock, this formation is structurally very heterogeneous with ubiquitous fractures and with mechanical properties defined by its bedding planes (Roggenthen & Doe, 2018; Ulrich et al., 2018). Besides the experimental work underground, the current state of the

[*] J. Ajo-Franklin, S.J. Bauer, T. Baumgartner, K. Beckers, D. Blankenship, A. Bonneville, L. Boyd, S.T. Brown, J.A. Burghardt, T. Chen, Y. Chen, K. Condon, P.J. Cook, P.F. Dobson, T. Doe, C.A. Doughty, D. Elsworth, J. Feldman, A. Foris, L.P. Frash, Z. Frone, P. Fu, K. Gao, A. Ghassemi, H. Gudmundsdottir, Y. Guglielmi, G. Guthrie, B. Haimson, A. Hawkins, J. Heise, C.G. Herrick, M. Horn, R.N. Horne, J. Horner, M. Hu, H. Huang, L. Huang, K. Im, M. Ingraham, T.C. Johnson, B. Johnston, S. Karra, K. Kim, D.K. King, T. Kneafsey, H. Knox, J. Knox, D. Kumar, K. Kutun, M. Lee, K. Li, R. Lopez, M. Maceira, N. Makedonska, C. Marone, E. Mattson, M.W. McClure, J. McLennan, T. McLing, R.J. Mellors, E. Metcalfe, J. Miskimins, J.P. Morris, S. Nakagawa, G. Neupane, G. Newman, A. Nieto, C.M. Oldenburg, W. Pan, R. Pawar, P. Petrov, B. Pietzyk, R. Podgorney, Y. Polsky, S. Porse, S. Richard, B.Q. Roberts, M. Robertson, W. Roggenthen, J. Rutqvist, D. Rynders, H. Santos-Villalobos, M. Schoenball, P. Schwering, V. Sesetty, A. Singh, M.M. Smith, H. Sone, C.E. Strickland, J. Su, C. Ulrich, N. Uzunlar, A. Vachaparampil, C.A. Valladao, W. Vandermeer, G. Vandine, D. Vardiman, V.R. Vermeul, J.L. Wagoner, H.F. Wang, J. Weers, J. White, M.D. White, P. Winterfeld, T. Wood, H. Wu, Y.S. Wu, Y. Wu, Y. Zhang, Y.Q. Zhang, J. Zhou, Q. Zhou, M.D. Zoback

art in coupled geomechanical modelling codes are being evaluated through forecasting exercises (White et al., 2019). These forecasting exercises are based on comprehensive structural and mechanical assessment of the stress condition, pre-existing fracture network (Dobson et al., 2018) and properties of the in-situ rock.

2. SEISMIC MONITORING ARRAY

The microseismic monitoring array was designed with the goal to deliver sensitive monitoring by small distances between the injection well and the receivers. Furthermore, it was anticipated that seismic events produced during the hydraulic fracturing stimulations would be of very high frequency. The six monitoring boreholes were instrumented with two strings of 12 hydrophones (HTI-96-Min) spaced 1.75 m and 18 3-component piezoelectric accelerometers (PCB 356B18), with three accelerometers deployed in each of the six monitoring boreholes (Figure 1). Additionally, four 3-component geophones were deployed in sub-vertical jackleg-drilled holes. Other monitoring systems deployed in the monitoring boreholes include 20 automated seismic sources for continuous active source seismic monitoring (CASSM) (Daley et al., 2007), a fiber-optic cable for distributed temperature sensing (DTS), distributed strain sensing (DSS), and distributed acoustic sensing (DAS), a 3-D electrical resistivity tomography array (Johnson et al., 2019) and thermistors for high precision temperature sensing. All sensors and active sources were attached to a 1-inch PVC pipe for conveyance using electrical tape and cable ties (Figure 2) and grouted in place. The injection and production boreholes were additionally instrumented with 3-component borehole deformation sensors (Guglielmi et al., 2014). The probe in the production borehole also included an array of conductivity sensors to precisely record the fracture breakthrough location in E1-P.

The signals were recorded on a total of three digitizers and acquisition systems. The first system is a set of four Geometric Geode seismic recorders for a total of 96 channels and operating at 48 kHz sampling rate. The system operates in triggered mode to record the CASSM surveys and was not used for microseismic analysis. A second system (OYO GeoRes) is a conventional 96 channel exploration seismograph and was operating in continuous mode and at 4 kHz sampling rate. Due to the relatively low sampling rate, no useful signal was recorded. The third system is a high-performance 64 channel digitizer (Data Translation VibBox) sampling sensors at 100 kHz with a 24 bit dynamic range. Due to the limited number of available channels, only the hydrophones and 12 of the 18 accelerometers were sampled by the VibBox unit. Four channels are reserved for the time signal and monitoring the CASSM system. It produces a data rate of about 25 MB/s which is stored on 8 TB hard drives that are replaced every three days. Data from this system was used for microseismic analysis described in this paper. The heavily instrumented experimental site provided its challenges which include uncertainty of the trajectories of the monitoring boreholes with impacts on the station coordinates. Further, we observed heavy electrical cross-talk between the electrical resistivity tomography system and the seismic recordings.
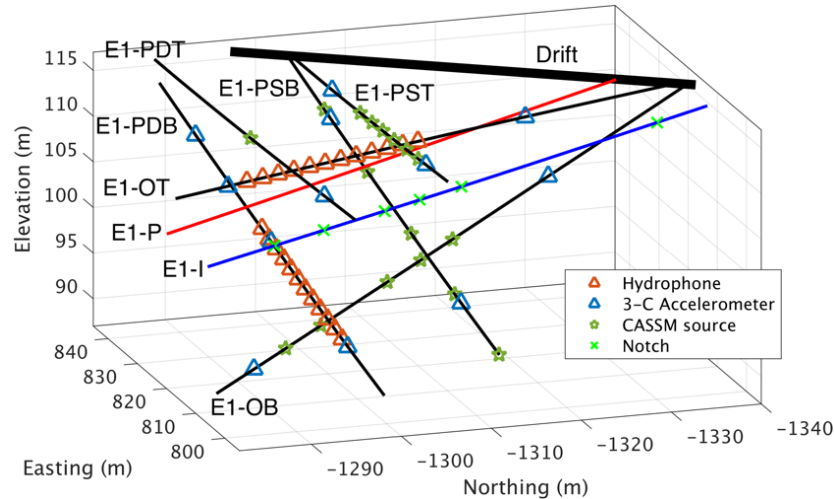

Figure 1: Seismic monitoring setup and notch locations used for stimulation.

3. PROCESSING

The raw data is processed using a lightweight Python processing stack based on the ObsPy package (Krischer et al., 2015). Events are detected using a coincidence STA/LTA trigger and first-motion P-wave arrivals are determined using an AIC picker (Chen & Holland, 2016). This system can process the incoming data stream on a single core in pseudo-realtime in the absence of recorded activity. If triggers are found, the processing becomes more complex due to the picking algorithm; distributed processing on several cores is required to keep up with the incoming data streams. We installed an 8-core workstation onsite which is able to provide near-realtime locations during ongoing stimulations depending on the level of activity.

Example waveforms from a subset of the accelerometers are shown in Figure 3. For some sensors (or source-receiver pairs), we typically record a strong and impulsive S-wave arrival. For others it may be harder to interpret as it is buried in the P-wave coda with complex scattering. A spectrogram is shown in Figure 4. Note the energy content of the event ranges from about 5 to 40 kHz. Energy observed above 20 kHz is above the specified response function of the accelerometers and may lead to resonance, complicating quantitative analysis.
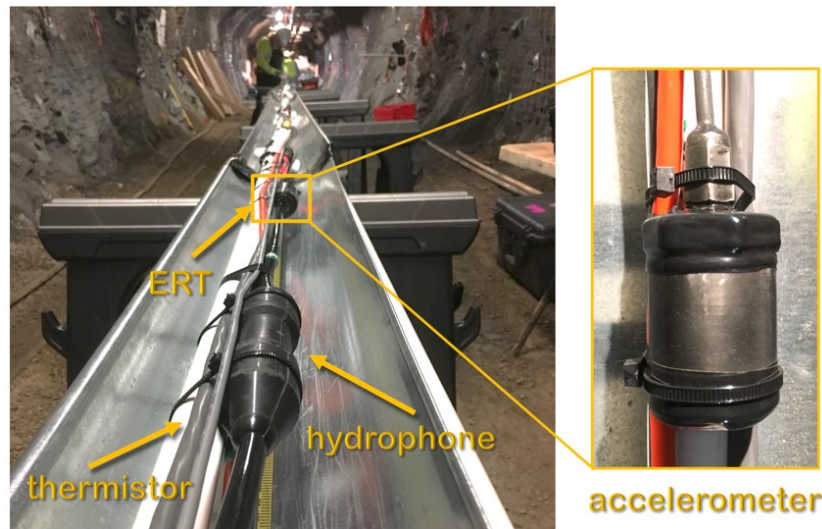
Figure 2: Assembly of monitoring strings with hydrophones and accelerometers fastened to PVC conveyance pipes using cable ties and electrical tape.
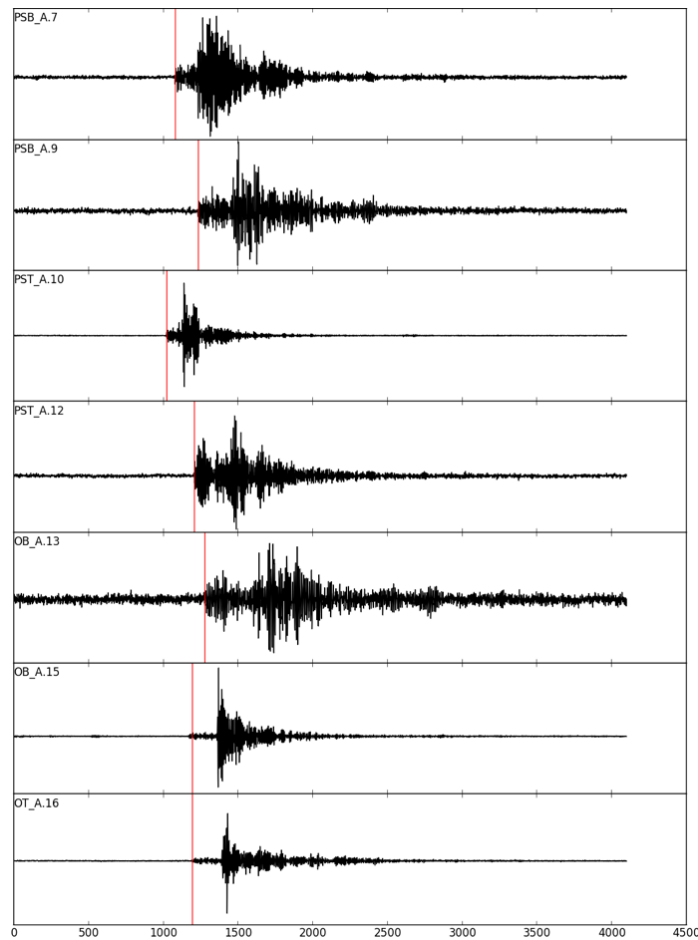

Figure 3: Sample waveforms of a typical, well-recorded event with automatic P-wave picks (red lines). Timeline is in samples where 1000 samples = 0.01 s.

For selected periods during active stimulation and flow tests, we manually review and refine the automatic P-wave picks and add S-wave picks. Events are located using a modified version of Hypoinverse (Klein, 2014) and a constant V_p of 5900 m/s and a V_p/V_s ratio of 1.78. The processing flow was also tested by locating the seismic sources. These sources, deployed at recorded points along the monitoring strings, were typically determined to be within 1 m of the known location. Incorporating a 3-D velocity model obtained from a seismic campaign (Schwering et al., 2018) will be a future step.
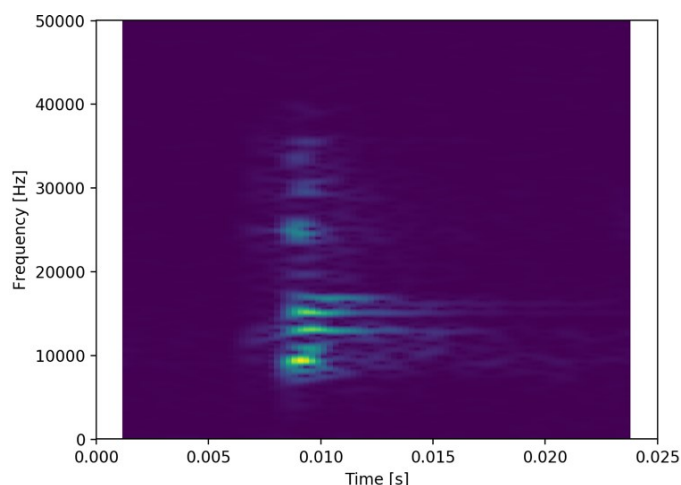
Figure 4: Spectrogram of OB_A.15 trace after applying filters as described in the text.

4. RESULTS

Stimulations and flow testing were performed on a series of notched locations. The first notch at 142 ft was abandoned after the first two short injection tests indicated that we reactivated a pre-existing natural fracture. The second notch at 164 ft depth was stimulated several times to grow the hydraulic fracture to larger size. The later flow tests and tracer characterization were performed from this location and it will be the major subject of this paper. At the end, we will discuss the injection in another notch at 128 ft depth.

Stimulation tests at the 164 ft notch started on May 22, 2018 (Figure 5). The first test lasted about 10 minutes at fracturing pressures of 23.1 to 25.5 MPa (3350 to 3700 psi) and an injection rate of ~200 ml/min. This test was designed to create a 1.5 m radius fracture ("Drive fracture to 1.5 m"). The E1-I well was shut-in for the night and stimulation continued to grow the fracture to a 5 m radius (calculated nominal value based on idealized geometry) during a circa 1 hour injection at 400 ml/min and pressures of around 25.9 MPa (3750 psi) ("Drive fracture to 5 m"). After another night of shut-in the injection continued at a higher rate (5000 ml/min) until the fracture hit the production well as determined from measured strain, decreased conductivity of the water and finally flow out of E1-P ("Drive fracture to E1-P"). The following day two flow tests were performed that also caused numerous microseismic events.

Drive to 1.5 m test

During the first stimulation at the 164 ft notch (Figure 6a), the pressure increased linearly to about 21.1 MPa (3060 psi) before we observed some yielding followed by a breakdown pressure of 24.1 MPa (3500 psi). Until then, only two microseismic event triggers were recorded (Figure 6b). Both triggers do not have clear impulsive arrivals and we could not determine a location for these. During
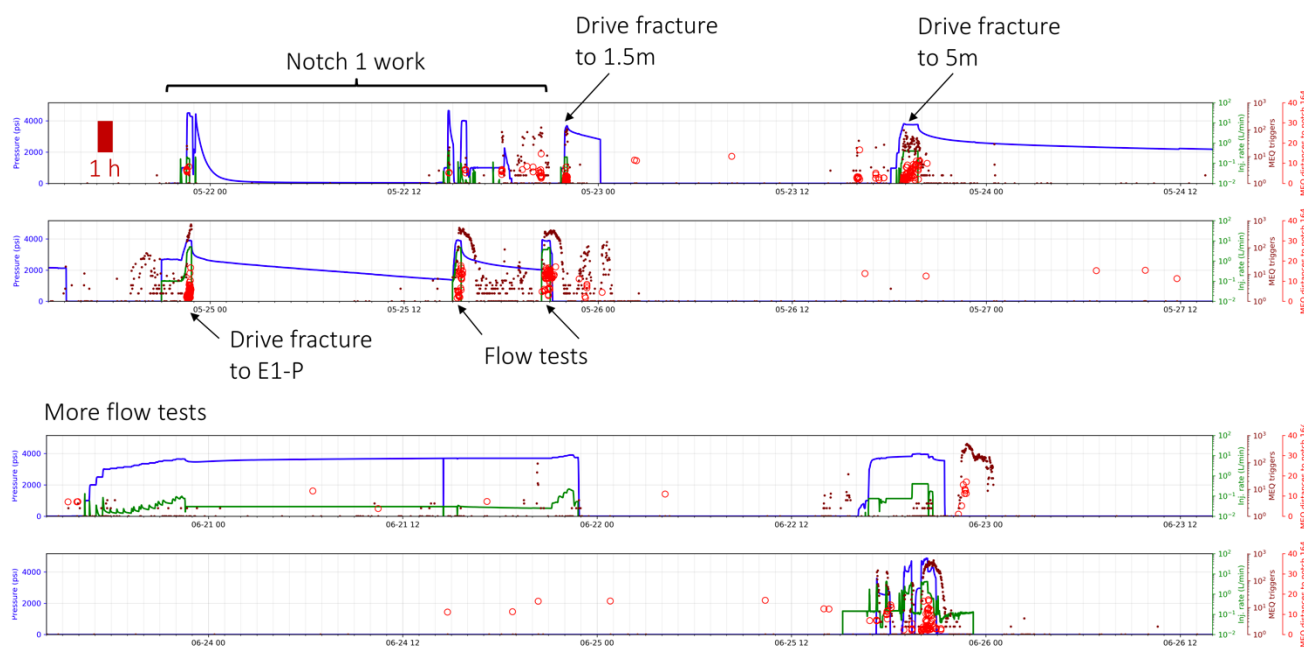

Figure 5: Summary of stimulations and flow tests performed on the notch at 164 ft. The MEQ triggers (brown dots) are counts of triggering events per minute. The MEQ distance to notch 164 (red circles), in meters, is the distance to the notch being stimulated.

4

the phase from reaching breakdown pressure at approx. 21:56:00 UTC to the local pressure minimum at approx. 21:56:40 UTC we observed only minimal microseismic activity. It is only afterwards as the pressure increased again that we observed abundant microseismic activity. Most microseismic activity during this initial test was located close to the injection borehole. The spatial distribution is too small to reliably identify trends that could be interpreted as a distinct structure.

Drive to 5 m test

During the next test, we injected sufficient fluid to grow the fracture to a large enough size so we could effectively image it with the microseismic array. To refine the event locations, we use the double difference method using the software HypoDD (Waldhauser & Ellsworth, 2000). Here we make use of the large source-receiver distance relative to the inter-event distances. The fracture started growing as a one-sided fracture towards the E1-P borehole but also with a strong upward component so it eventually connected up with the E1-OT borehole. In Figure 7 a summary of the temporal evolution is shown. Although the event density is not very high, we can extrapolate that the microseismic event reached the E1-OT borehole around 19:30 UTC (Figure 7a). At this time the envelope of the microseismic event front reached about 10 m (Figure 7b). The DTS system (sampling every 15 min) recorded a temperature anomaly starting around 19:30 UTC as well at a depth of 44 m, which is consistent with the microseismic event locations (Figure 7c).
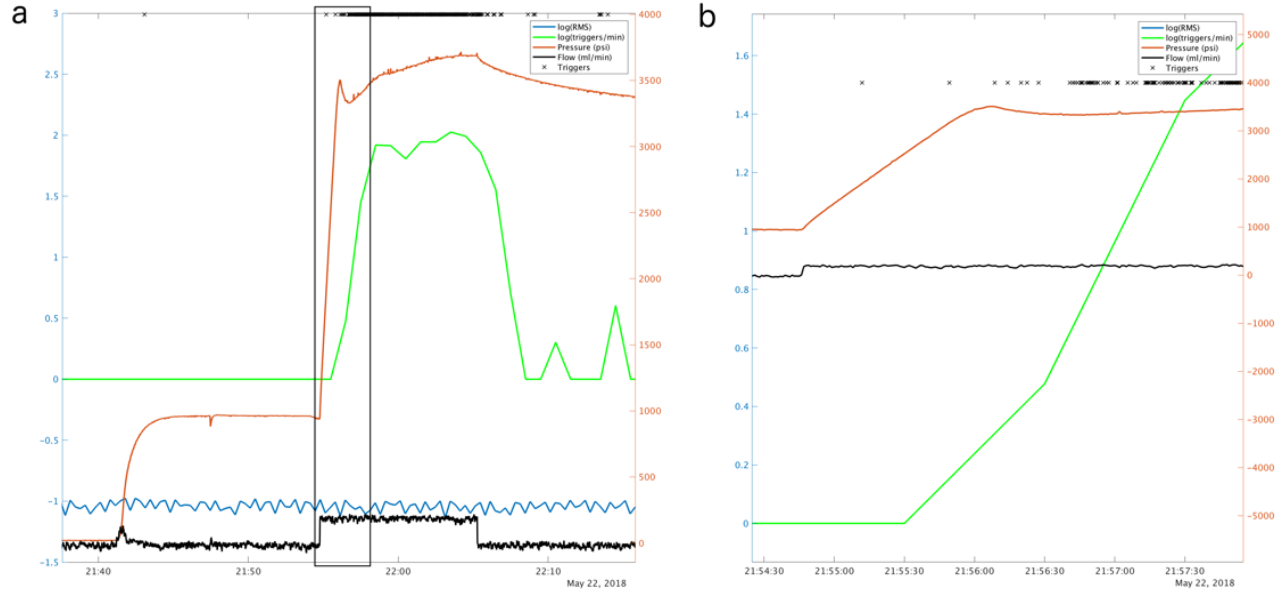

Figure 6: Hydraulic parameters (pressure in orange, injection rate in black) and microseismic event triggers (number of triggers per minute in green and distinct triggers as black crosses) for the 1.5m injection test. (b) is a zoom into the early part of the stimulation as outlined by the box in subfigure (a).
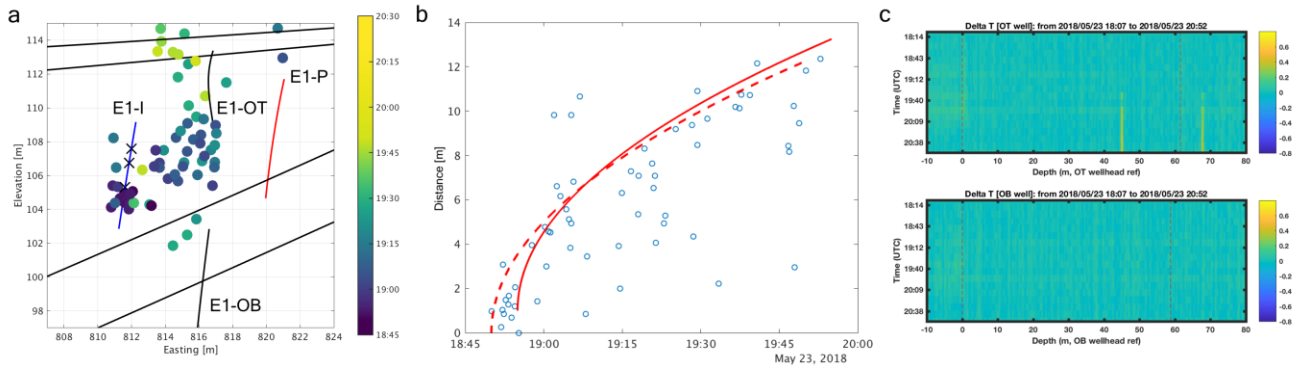

Figure 7: Fracture growth during the "Drive to 5 m" stimulation with intersection points in the E1-OT borehole and temperature anomaly recorded in the DTS system at around 19:30 UTC. Figure (a) shows the seismicity in an along-borehole-axis view of E1-I. The occurrence time of microseismicity is color-coded. Black lines are borehole trajectories. Figure (b) shows the distance of microseismic events from the stimulated notch with two envelopes of sqrt(t) shown. The origin of the parabolas is the time of the first event (dashed) and of the beginning of fracture propagation away from E1-I (solid), respectively. Figure (c) shows the temperature anomaly in the borehole E1-OT measured on the DTS system at 45 m (down-going fiber strand) and 68 m (up-going fiber strand) and beginning around 19:30 UTC.

Overall activity

Figure 8 shows the overall activity recorded during periods of active injection in the 164 ft notch as shown in Figure 5. The main trend of seismicity is oriented sub-parallel to the direction of S_{HMax} (Dobson et al., 2018), however there is a large amount of structural complexity. We observe two off-shooting planar features (fractures 6 and 7 in Figure 9) intersecting the main trend at the injection borehole and about 3 m east of the injection borehole, respectively. During later injections, structures detached from the main trend were active. Overall, we could interpret 6 fracture planes from the microseismic event locations from Notch 2 injections (Figure 9). The trend of activity parallel to E1-I is interpreted as near-wellbore activity. The observed systematic offset relative to the injection well may indicate heterogeneities of the velocity and uncertainties in the trajectories of boreholes.
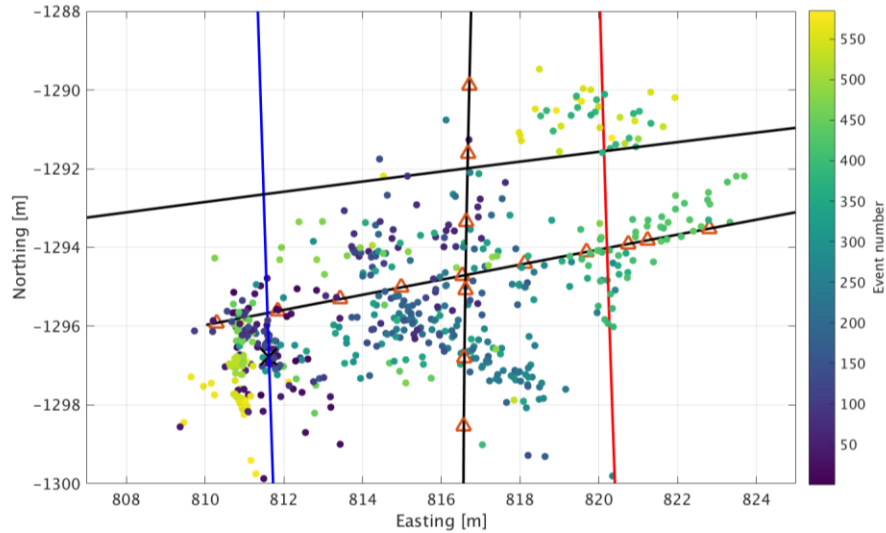

Figure 8: MEQ locations color-coded by order of occurrence. Injection borehole E1-I in blue, production borehole E1-P in red, the 164 ft notch is marked by the black cross. Triangles are locations of hydrophones and accelerometers.

Stimulation of Notch 128 ft

A third notch at 128 ft was stimulated in July 2018. We recorded much less activity than during the previous tests. In order to image the activated fractures properly, we relied on manual reprocessing to obtain phase arrivals from even smaller events than for the previous tests. In total we could detect and locate 156 events during the initial stimulation and subsequent flow test, with most events occurring during the flow test. Located events are distributed over two planar features at a shallow angle with the injection borehole (Figure 9). The orientations of these features are very different from the one activated during the injections at the 164 ft notch and not compatible with the creation of a hydraulic fracture. This is despite the higher fracture propagation pressure of around 27.6 MPa (4000 psi), that was observed for the stimulation at the 128 ft notch. The shallow dipping planes could be independently confirmed by DTS which determined a fracture intercept with the E1-OT borehole at shallow depth through a temperature anomaly in agreement with the microseismic cloud.
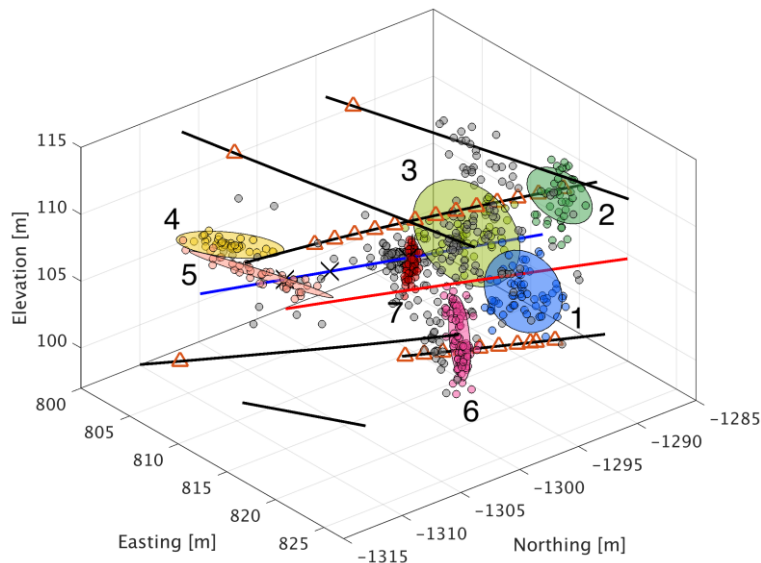

Figure 9: Fracture planes identified from MEQ locations.

Fracture network

To quantitatively analyze the reactivated fracture planes, we manually interpret the cloud of located events for planar features. For the planes active during flow at the 164 ft notch we determined a series of steeply dipping planes with dips ranging from 75° to 88°. The planes active during the 128 ft notch injections have much shallower dip angles of 16° and 36°, respectively.

4. CONCLUSIONS

We have recorded meso-scale hydraulic fracturing tests with a novel 100 kHz, continuous monitoring system deployed in six monitoring boreholes surrounding the experimental domain in 3-D. The accelerometers and hydrophones allowed very sensitive detections with a large number of microseismic events in the frequency band from 3 to 40 kHz. The recorded main trend of seismicity agrees well with independent measurements of the intercepting hydraulic fractures with other boreholes. The stimulations at the 164 ft notch intercepted borehole E1-OT, with time and location confirmed by temperature anomalies recorded by the DTS system, and borehole E1-P, with time and location confirmed by 3-D strain and distributed fluid conductivity measurements. Although we identified several strands of activated fracture planes, they agree with the hypothesis of hydraulic fractures parallel to the S_{HMax} direction. The slightly varying orientation of fractures could be explained by structural heterogeneity of crystalline rock (Schoenball & Davatzes, 2017). Additionally, we identified two off-shoot structures which agree with the structural fabric and may represent reactivation of pre-existing structures. The stimulations at the 128 ft notch activated very different structures with shallow dips. They were confirmed by temperature anomalies recorded in E1-OT. The orientation of these planes was unexpected and is not compatible with hydraulic fractures in the same stress field as the features activated at the 164 ft notch. Fu et al. (2019) provide a complementary interpretation of the microseismic locations, incorporating additional information from flow zones identified through sewer camera images during flow tests. Further efforts on analysis of the microseismic data include cross-correlation techniques to identify event clusters (Templeton et al., 2019) and novel detection and location techniques (Chen et al., 2019).

REFERENCES

Chen, C., & Holland, A. A. (2016). PhasePApy: A Robust Pure Python Package for Automatic Identification of Seismic Phases. *Seismological Research Letters*, *87*(6), 1384–1396. https://doi.org/10.1785/0220160019

Chen, Y., Huang, L., Schoenball, M., Ajo-Franklin, J., Kneafsey, T. J., & EGS Collab Team. (2019). Real-Time Microearthquake Event Detection and Location in Anisotropic Media Using a Multiscale Scanning Approach for EGS Collab Experiments. In *Proceedings 44th Workshop on Geothermal Reservoir Engineering, Stanford University*.

Daley, T. M., Solbau, R. D., Ajo-Franklin, J. B., & Benson, S. M. (2007). Continuous active-source seismic monitoring of C O2 injection in a brine aquifer. *GEOPHYSICS*, *72*(5), A57–A61. https://doi.org/10.1190/1.2754716

Dobson, P., Kneafsey, T., Morris, J., Singh, A., Zoback, M., Roggenthen, W., … EGS Collab Team (2018). The EGS Collab hydroshear experiment at the Sanford Underground Research Facility – Siting criteria and evaluation of candidate sites. *Geothermal Resources Council Transactions* 42, 708–723.

Frash, L. P., Carey, J. W., Welch, N. J., & EGS Collab Team. (2019). EGS Collab Experiment 1 Site Geomechanical and Hydrological Properties by Triaxial Direct Shear. In *Proceedings 44th Workshop on Geothermal Reservoir Engineering, Stanford University*.

Fu, P., Schoenball, M., Morris, J., Ajo-Franklin, J., Knox, H. A., Kneafsey, T. J., … EGS Collab Team. (2019). Microseismic Signatures of Hydraulic Fracturing: A Preliminary Interpretation of Intermediate-Scale Data from the EGS Collab Experiment. In *Proceedings 44th Workshop on Geothermal Reservoir Engineering, Stanford University*.

Guglielmi, Y., Cappa, F., Lançon, H., Janowcsyk, J. B., Rutqvist, J., Tsang, C.-F., & Wang, J. S. Y. (2014). ISRM Suggested Method for Step-Rate Injection Method for Fracture In-Situ Properties (SIMFIP): Using a 3-Components Borehole Deformation Sensor. *Rock Mechanics and Rock Engineering*, *47*(1), 303–311. https://doi.org/10.1007/s00603-013-0517-1

Johnson, T. C., Strickland, C., Vermeul, V., Mattson, E., Knox, H. A., Ajo-Franklin, J., … EGS Collab Team. (2019). EGS Collab Project Electrical Resistivity Tomography Characterization and Monitoring. In *Proceedings 44th Workshop on Geothermal Reservoir Engineering, Stanford University*.

Klein, F. W. (2014). *User's Guide to HYPOINVERSE-2000, a Fortran Program to Solve for Earthquake Locations and Magnitude* (U. S. Geological Survey, Open File Report 02-171, revised June 2014).

Kneafsey, T. J., Blankenship, D., Knox, H. A., Johnson, T. C., Ajo-Franklin, J., Schwering, P. C., … EGS Collab Team. (2019). EGS

Collab Project: Status and Progress. In *Proceedings 44th Workshop on Geothermal Reservoir Engineering, Stanford University*.

Krischer, L., Megies, T., Barsch, R., Beyreuther, M., Lecocq, T., Caudron, C., & Wassermann, J. (2015). ObsPy: a bridge for seismology into the scientific Python ecosystem. *Computational Science & Discovery*, *8*(1), 014003. https://doi.org/10.1088/1749-4699/8/1/014003

Morris, A., Ferrill, D. A., & Brent Henderson, D. B. (1996). Slip-tendency analysis and fault reactivation. *Geology*, *24*(3), 275. https://doi.org/10.1130/0091-7613(1996)024<0275:STAAFR>2.3.CO;2

Oldenburg, C. M., Dobson, P. F., Wu, Y., Cook, P., Kneafsey, T. J., Nakagawa, S., … Heise, J. (2017). Hydraulic Fracturing Experiments at 1500 m Depth in a Deep Mine: Highlights from the kISMET Project. In *Proceedings 42th Workshop on Geothermal Reservoir Engineering, Stanford University* (p. 9).

Roggenthen, W., & Doe, T. (2018). Natural Fractures and Their Relationship to the EGS Collab Project in the Underground of the Sanford Underground Research Facility (SURF). In *52nd US Rock Mechanics / Geomechanics Symposium, Seattle* (p. 11).

Schoenball, M., & Davatzes, N. C. (2017). Quantifying the heterogeneity of the tectonic stress field using borehole data. *Journal of Geophysical Research: Solid Earth*, *122*(8), 6737–6756. https://doi.org/10.1002/2017JB014370

Schwering, P. C., Knox, H. A., Hoots, C. R., Linneman, D., Ajo-Franklin, J., & EGS Collab Team. (2018). The EGS Collab Hydrofracture Experiment at the Sanford Underground Research Facility – Campaign Cross-Borehole Seismic Characterization. *GRC Transactions*, *42*, 10.

Templeton, D., Morris, J., Schoenball, M., Wood, T., Robertson, M., Cook, P., … EGS Collab Team. (2019). Microseismic Correlation and Relocation Analysis of DOE EGS Collab Data. In *Proceedings 44th Workshop on Geothermal Reservoir Engineering, Stanford University*.

Ulrich, C., Dobson, P. F., Kneafsey, T. J., Roggenthen, W., Uzunlar, N., Doe, T., … EGS Collab Team. (2018). The distribution, orientation, and characteristics of natural fractures for Experiment 1 of the EGS Collab Project, Sanford Underground Research Facility. In *52nd US Rock Mechanics / Geomechanics Symposium, Seattle* (p. 8).

Waldhauser, F., & Ellsworth, W. L. (2000). A Double-Difference Earthquake Location Algorithm: Method and Application to the Northern Hayward Fault, California. *Bulletin of the Seismological Society of America*, *90*(6), 1353–1368. https://doi.org/10.1785/0120000006

White, M. D., Fu, P., Ghassemi, A., Huang, H., Rutqvist, J., Johnston, B., … EGS Collab Team. (2019). The Necessity for Iteration in the Application of Numerical Simulation to EGS: Examples from the EGS Collab Test Bed 1. In *Proceedings 44th Workshop on Geothermal Reservoir Engineering, Stanford University2*.